Graft polymerization of ε-caprolactone to cellulose nanocrystals and optimization of grafting conditions utilizing a response surface methodology

Chen Tian, Shiyu Fu*, Jianhao Chen, Qijun Meng, and Lucian A. Lucia

KEYWORDS: Poly(ε-caprolactone), Cellulose Nanocrystals, Grafting, Statistical Optimization

SUMMARY: The objective of this study was the grafting, statistical polymerization optimization, and subsequent characterization of poly(ε-caprolactone)grafted cellulose nanocrystals (CNCs) obtained by ring opening polymerization. The most significant variables on the grafting ratio of poly(\varepsilon-caprolactone) as obtained from the response surface methodology (Box-Behnken content, polymerization were monomer temperature, and polymerization time. It was shown that an experimental grafting ratio of 134.23% closely matched the predicted rate of 138.57%, within an R^2 =99.79% under the proposed optimized conditions. The optimum operating conditions obtained from the response surface methodology were the following: εcaprolactone: CNCs mass ratio (monomer content) of 14:1, polymerization temperature of 130°C and polymerization time of 26.5 h. It was shown that poly(εcaprolactone) successfully grafted onto the cellulose nanocrystals while cellulose nanocrystals maintained their original morphology and their native crystallinity. Although, the surface coverage was relatively low, the poly(ε-caprolactone)-grafted nanocellulose was shown to be much more hydrophobic compared to unmodified cellulose nanocrystals.

ADDRESSES OF THE AUTHORS: Chen Tian (birdytc@hotmail.com), Shiyu Fu (shyfu@scut.edu.cn), Jianhao Chen (pk_hao@hotmail.com), Qijun Meng (Moon647@126.cn): State Key Laboratory of Pulp and Paper Engineering, South China University of Technology, Guangzhou, 510640, China, Lucian A. Lucia (lalucia@ncsu.edu): Department of Forest Biomaterials, Department of Chemistry, NC State University, Raleigh, NC, USA

Corresponding authors: Shiyu Fu Present address: State Key Laboratory of Pulp and Paper Engineering, South China University of Technology, Guangzhou, 510640, China (shyfu@scut.edu.cn)

Lucian A. Lucia Present address: Department of Forest Biomaterials, Department of Chemistry, NC State University, Raleigh, NC, USA (lalucia@ncsu.edu)

The ever increasing attention to global environmental sustainability coupled with the concurrent depletion of fossil resources provide a platform on which nanocellulose gains ascendancy as a potential solution to the latter issues (Goffin et al. 2011a). There are several types of nanocellulose that provide avenues for new product platforms such as nanofibrillated cellulose (NFC), cellulose nanocrystals (CNCs), and bacterial nanocellulose (BNC) (Klemm et al. 2005). CNCs are a natural material derived from cellulose and display high

reactivity, biodegradability, renewability, and natural abundance (Habibi et al. 2010). They are a highly crystalline type of cellulose that have a rod-like structure with an average length of ~100 nm and a diameter of ~10 nm, measurements that are generally dependent on the cellulose source. In addition, CNCs have a large surface area, high crystallinity, and high strength. These latter highly attractive properties are extremely useful for contributing to an increase in the mechanical performance of composites especially when the CNCs are doped at low levels (less than 5 wt-%). In fact, a great fraction of the recent work with CNCs has focused on its application as reinforcing filler in nanocomposite materials (Cao et al. 2009, Wang et al. 2010, Zhou et al, 2012). The resulting tended to nanocomposites display outstanding mechanical properties in terms of both stiffness and thermal stability. Peng incorporated NFC into xylan-rich hemicelluloses (XH) to prepare composite films (Peng et al. 2011). The incorporation of NFC into the films enhanced the mechanical properties because of the intrinsic mechanical strength of the NFC and strong interactions between it and the XH matrix. Wu prepared a much more superior strength (with respect to stiffness and thermal stability) elastomeric nanocomposite by dispersing microcrystalline cellulose into a polyurethane matrix (Wu et al. 2007).

The most important hurdle to overcome when considering cellulose nanocrystals as a possible reinforcement filler within nanocomposites is the poor compatibility between hydrophilic CNCs and the typically hydrophobic polymer matrices (Dufresne 2003, Roman et al. 2006). Another hurdle that prevents CNC incorporation into hydrophobic matrices irreversible agglomeration of CNCs as result of strong hydrogen bonds after drying. These latter two hurdles make it difficult to reliably and effectively disperse CNCs in a hydrophobic matrix or in any common nonpolar solvent (Samir et al. 2005). To overcome the inherent incompatibility of CNCs/hydrophobic/nonpolar solvent systems, researchers have attempted to reduce the surface energy of CNCs by introducing hydrophobic brushes (surface groups) onto the surface. The chemical approaches to introduce such groups are the following: reversible addition-fragmentation chain transfer (RAFT) polymerization (Liu et al. 2010), ring-opening polymerization (ROP) (Labet, Thielemans 2011), and atom transfer radical polymerization (ATRP) (Morandi et al. 2009). The ROP method is one of the more common ways for addressing cellulose modification (Carlmark et al. 2012). Dong prepared cellulose-g-PLA copolymers by ROP of L-lactide (LA) with cellulose in an ionic liquid, [Amim]Cl (Dong et al. 2008). Goffin successfully grafted PCL-b-LA diblock copolymers onto the surface of CNCs

by ROP (Goffin et al. 2012). They found that the modified cellulose become more hydrophobic.

Poly(ε-caprolactone) (PCL)is a hydrophobic polyester with a low glass transition temperature. It is biocompatible and biodegradable with good mechanical properties. Thus, PCL is particularly interesting as a potential matrix compatibilizer for CNC-based nanocomposites. Grafting PCL to various cellulose substrates via ROP has already been widely investigated. Lönnberg grafted PCL to microfibrillated cellulose and studied the thermal behavior, crystallization, and melting behavior of the resultant nanocomposite (Lönnberg et al. 2008). She found that this approach made it possible to obtain a stable dispersion of MFC in a nonpolar solvent. Habibi prepared nanocomposites that possessed a high grafting density of high MW PCL to CNCs (Habibi et al. 2008). Goffin also dispersed PCL-grafted CNCs within a commercial poly(e-caprolactone) matrix and studied the thermo-mechanical properties of the resultant matrices (Goffin et al. 2011b). They found that the interfacial compatibility between the modified cellulose and the matrix was excellent and that the thermo mechanical and rheological performances of the composites were largely enhanced. However, recent studies on PCL-modified nanocellulose have mainly focused on its ability to provide reinforcement to the hydrophobic matrix. To this point, very few studies on both of the grafting and polymerization optimization strategies of monomers onto nanocellulose have been achieved. Such studies would undoubtedly assist in the future development of nanocomposites if the factors controlling the overall modification of the surface of CNCs were well elucidated.

Conventionally, modification approaches of CNCs are optimized by using a 'one-at-a-time strategy' for the reaction parameters. However, this approach is time consuming and often leads to misinterpretation of results when there is a possibility of interactions among the different components. In recent years, the use of a statistical approach involving Plackett-Burman design and response surface methodology (RSM) has gained significant attention for the optimization of the medium and for understanding the interactions among various parameters by introducing a minimum number of experiments (Siala et al. 2012). Carbone prepared a type of cationic solid lipid nanoparticle (SLN), and optimized the process by a full factorial experimental design to study the effects of two independent variables (amount of DOTAP and concentration of the lipid matrix) and their interaction on mean particle size and zeta potential values (Carbone et al. 2012). Hajji maximized alkaline protease production by screening the main factors using a Plackett-Burman design, and assessing the optimal region for the significant variables using RSM (Hajji et al. 2008).

RSM, including the Box-Behnken design (BBD) and the central composite design (CCD), is a collection of statistical techniques for designing experiments, evaluating the effects of factors, and searching optimum conditions of factors on responses (Coninck et al. 2000). The factorial analysis of RSM gives the maximum amount of information from the experimental data and

will establish the influence of multiple factors on the formulation properties (Vitorino et al. 2011). RSM has been successfully applied in many topical areas including biotechnology (Imandi et al. 2008, Mohana et al. 2008), degradation (Ghanem et al. 2009, Zhou et al. 2011), fermentation (Açıkel et al. 2010), and synthesis (Hadidi et al. 2011). For example, Wang studied the optimization of coagulation-flocculation in pulp mill wastewater treatment using a combination of uniform design and response surface methodology (Wang et al. 2011). Fu used RSM to investigate the effect of operation conditions on photo-electrocatalytic oxidation of fulvic acid (Fu et al. 2007). However, no studies have been reported on the optimization of factors and their interactions for improving the grafting efficiency of nanocellulose by ROP.

Therefore, the current work focuses on the systematic grafting of PCL to CNCs via ROP, including optimization of the polymerization (i.e., monomer content, polymerization temperature, polymerization, and time) and the characterization of the resultant PCL-g-CNCs. An attempt has been made to employ RSM to optimize the key parameters on the grafting efficiency.

Materials and Methods

Materials

Cotton linter with a moisture content of 8% was used as obtained. Sulfuric acid (98%), acetone (99%), toluene (anhydrous, 99.8%), 4-dimethylamiopryidine (DMAP) (98%), tartaric acid(99%) dichloromethane (99.5%), were all laboratory grade and obtained from Guangzhou Chemical Reagent Factory (Guangzhou, China). \(\varepsilon\)-caprolactone (\varepsilon\)-CL) and Sn(Oct)2 (98%) were obtained from Aladdin Industrial, Inc. (Shanghai, China). Toluene was dried using metal sodium and distilled before use. Acetone was dried using potassium permanganate and distilled before use. \(\varepsilon\)-caprolactone was dried 48 h over calcium hydride, distilled under reduced pressure prior to use, and stored under nitrogen atmosphere. Other chemicals were used without further purification.

Cellulose nanocrystal preparation

Following the previous work from this lab (Zhou et al. 2012), approximately 3 g of cotton linters (dry weight) was mixed with sulfuric acid (64 wt-%), and the mixture was hydrolyzed at 45°C for 90 min. under continuous mechanical stirring (500 rpm). The hydrolysis was quenched by adding 500 ml of water to the reaction mixture and then the slurry was washed with distilled water for 20 min. at 5000 rpm, using repeated centrifugation. The centrifugation step continued until the pH of the supernatant was 1. The last wash was conducted using dialysis with distilled water until the wash water maintained pH 7. The resultant suspension was stored at 4°C before further analysis or treatments.

Grafting of PCL to CNCs via ring-opening polymerization

An aqueous suspension containing 0.5 g of CNCs was pretreated by solvent-exchange or freeze-drying, and dispersed in dried toluene by ultrasonication. The toluene

Table 1 - Level and code of variables for RSM.

Variables	Symb	Levels			
variables	Uncoded	Coded	-1	0	1
Monomer content					
(mass ratio of ε-CL	X 1	X_1	4:1	12:1	20:1
to CNCs)					
Polymerization	X 2	χ_2	90	110	130
temperature (°C)	Λ2	712	50	110	100
Polymerization time	X 3	Хз	12	24	36
(h)	Α3	/\3	12		00

suspension was introduced into a dried three-neck flask having a magnetic stirrer. Toluene was distilled to remove residual water. The flask was heated to a 90°C under a blanket of nitrogen. ε-CL and 2 wt-% (with respect to the monomer) of the catalyst were slowly added into the solution. The polymerization was allowed to proceed for 24 h. After cooling to room temperature, the modified CNCs were recovered by precipitating the mixture into carbinol. Subsequently, the product was washed several times using dichloromethane and Soxhlet extracted for 48 h in dichloromethane to remove homo-PCL and unreacted ε-CL. The final product was dried in vacuum for 48 h at 45°C.

Response surface methodology

A Box-Behnken design with three main factors was employed for optimizing the reaction conditions. Grafting ratio (Gr) was selected as the dependent variable to represent the overall grafting efficiency that can be calculated according to Eq1:

$$Gr(\%) = \frac{m_1 - m_0}{m_0} \times 100$$
 [1]

where m_0 is the initial mass of CNCs before ROP, and m_1 is the final mass of PCL-g-CNCs after vacuum drying. In this research, the monomer content (mass ratio of ϵ -CL to CNCs) (X_1), polymerization temperature (X_2) and polymerization time were selected as the three independent variables. An empirical second-order polynomial model for the three factors was used to obtain the mathematical model:

$$Y = \beta_0 + \sum \beta_i X_i + \sum \beta_{ij} X_i X_j + \sum \beta_{ii} X_i^2$$
 [2]

In this equation, Y is the predicted response (Gr, %) used as a dependent variable; X_i (i=1,2 and 3) are the input predictors or controlling variables; and β_0 , β_i (i=1,2,3) and β_{ii} (i=1,2,3; j=1,2,3) are the model coefficient parameters (Fu et al. 2007). *Eq1* was applied for three responses to describe the principal effects and interaction among the identified variables. The minimum (coded as -1) and maximum (coded as +1) ranges of each variable were studied and the full experimental details for actual and coded values are listed in *Table 1*. The experimental results are shown in *Table 2*. Minitab 16 was used for both the design and statistical analysis of the experimental data. An analysis of variance (ANOVA) was used to estimate the statistical parameters.

Characterization

Fourier transform infrared analyses (FT-IR). The FT-IR traces of CNCs and PCL-g-CNCs were collected using a Bruker spectrometer (TENSOR27, Switzerland) in KBr discs. The sample was weighed and its mass ratio with

Table 2 - The design of RSM and its actual and predicted values

Run	Χ	Х	Х	Graftin	Grafting rate (%)		
Kuii	1	2	3	Experimental	Predicted		
1	0	1	1	130.40	127.8394		
2	-1	0	-1	35.00	34.04462		
3	-1	-1	0	24.30	22.71122		
4	0	0	0	121.00	122.5996		
5	0	0	0	123.62	122.5996		
6	1	1	0	110.40	112.2793		
7	0	-1	1	87.32	88.41018		
8	-1	1	0	52.80	55.02042		
9	0	-1	-1	75.26	78.11178		
10	0	1	-1	120.94	120.133		
11	-1	0	1	39.60	40.45502		
12	1	-1	0	65.08	63.1381		
13	1	0	-1	80.86	80.2955		
14	-1	0	0	122.76	47.54582		
15	1	0	1	90.66	91.8899		

KBr was 1:100. Spectra were recorded using a spectral width ranging from 400 to 4000 cm⁻¹.

X-ray diffraction (XRD). XRD was determined by a D/max-IIIA X-ray diffractometer, in which the high-intensity monochromatic nickel-filtered Cu Ka radiation was generated at 40 kV and 40 mA. Diffractograms were collected over a 2θ range of $4{\sim}60^{\circ}$ at a rate of 1° /min with a resolution of 0.04° at room temperature. The crystallinity (Cr) was evaluated using Eq 3.

$$Cr = \left[1 - \frac{IA}{IA + Sp}\right] \times 100\%$$
 [3]

Where IA is the amorphous integrated area, and Sp is the sum of the integrated areas of the 101, 101 and 002 peaks (He et al. 2008).

Thermogravimetric analysis (TGA). TGA was performed using a TA Instrument Q50 thermogravimetric analyzer (TGA Q500, TA, USA). Samples of approximately 10 mg mass were heated in an aluminum crucible to 600°C at a heating rate of 10°C/min while the apparatus was continually flushed with anitrogen flow rate of 25 ml min⁻¹.

Atomic force microscopy (AFM). AFM images were recorded using a Nanoscope IIIa Multimode microscope operating in tapping mode at room temperature under air. For nanocellulose observation, a droplet of the nanocellulose suspensions (0.01wt-%) was put on a fresh mica substrate. Commercial probes were used with a spring constant of 20e-80 N/m and a resonance frequency of about 298-335 kHz.

X-Ray photoelectron spectroscopy (XPS). Surface chemical composition of CNCs and CNC-g-PCL were analyzed by XPS. Powdered cellulose nanocrystals before and after PCL grafting were tested with a XPS instrument (Axis Ultra DLD, Kratos Analytical, UK). The monochromatic A1 K_a X-ray source was operated at 150 W and with an electron flood gun for charge compensation. The pass energy was 160 and 40 eV for low and high resolution spectra, respectively. The relative amounts of different bound carbons were determined

from high-resolution C1s spectra. A gaussian curve fitting program was used to treat the C1s signal. The spectra were modified by setting the C–C contribution in the C1s emission at 285.0 eV.

Contact angle. Contact angle measurements were performed at room temperature on a CAM 200 instrument (KCV Instrument, Ltd.). Smooth surface samples were obtained by compressing the powder under 10 metric tons pressure using a KBr press. A $5{\sim}10~\mu l$ volume droplet of ultrapure water was dispensed on the surface of the sample. Images of the droplet profile were recorded from which the CA was determined using the angle of intersection between a baseline and a circle.

Results and discussion

Screening of pretreatment methods

CNCs were first transported from aqueous suspension to toluene suspension using some pretreatment methods solvent-exchange protocol or freeze-drying. For solvent exchange, CNCs were exchanged by using an aqueous suspension, dried acetone, and finally dried toluene via several successive centrifugation and redispersion steps (Habibi et al. 2008). In the freeze-drying method, the CNC aqueous suspension was dried by freeze-drying for 24 h, and Soxhlet extracted for 48 h in ethanol to remove low molecular weight organic compounds adsorbed on the surface of CNCs (Labet et al. 2011). The purified CNCs were dried in vacuum for 48 h at 45°C and dispersed in toluene directly by ultrasonic dispersion. The two methods have been both previously used in other work (Giffin et al. 2012, Lönnberg et al. 2008). The FT-IR spectra of PCL-g-CNCs obtained by the two methods are displayed in Fig 1.

Compared to the unmodified CNCs (*Fig 1A*), the FT-IR spectrum (*Fig 1B*) of the PCL-g-CNCs obtained by solvent exchange shows new peaks at 1730 cm⁻¹ and 2905 cm⁻¹, which can be ascribed to the stretching frequency of the carboxyl groups and –CH₂– groups, respectively, from the grafted chains. Meanwhile, in the FT-IR spectrum of PCL-g-CNCs obtained from freezedrying (*Fig 1C*), the intensity of these signals were very weak, indicating that few PCL chains were grafted onto the surface of CNCs. It is found that the grafting

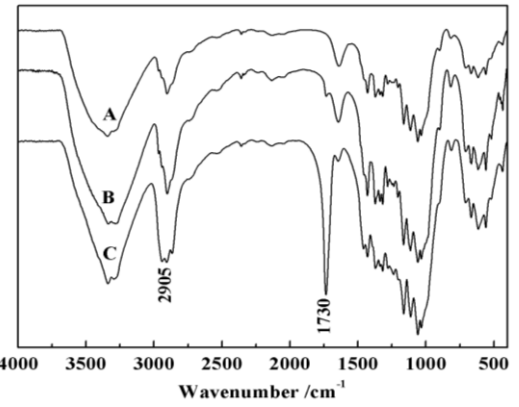


Fig 1 - The FT-IR spectra of CNCs and PCL-g-CNCs (A: CNCs; B: PCL-g-CNCs-solvent exchange protocol; C: PCL-g-CNCs-freeze-drying).

efficiency was to a large extent controlled more by the solvent exchange versus freeze-drying. Likely this is a function of the dispersibility of the CNCs. It is known, for example, that the CNCs in this work that were obtained from sulfate acid hydrolysis, provide self-repulsive forces that improve the suspension stability (Jiang et al. 2010). Therefore the solvent exchange method can maintain the stability and improve the dispersibility of CNCs in toluene. But for the freeze-drying protocol, freezing CNCs followed by sublimation of ice resulted in strong hydrogen bonds between CNCs, leading to large sheet-like aggregations of the colloidal suspension (Korhonen et al. 2011). These aggregations reduced the dispersibility of CNCs in toluene, and then adversely affected the reactivity of CNCs toward ROP.

Selection of catalysts

ROP of lactones is most commonly performed in the presence of a metal-based catalyst such as Sn(Oct)₂. However, organic catalysts have recently been applied to ε-CL polymerization. Guo found that the copolymers synthesized using DMAP as catalyst showed significantly higher grafting levels of PCL than those synthesized using Sn(Oct)₂ as catalyst (Guo et al. 2013). Hafrén (Hafrén et al. 2005) reported that tartaric acid was an efficient catalyst for the grafting. To obtain a useful comparison of the catalytic effect of Sn(Oct)₂ against new organic catalysts for the grafting polymerization of cellulose with ε-CL, three typical catalysts systems, Sn(Oct)₂, DMAP, and tartaric acid were studied in parallel. FT-IR spectrums of PCL-g-CNCs from the three catalysts are shown in *Fig* 2.

According to Fig 2, no PCL was grafted on CNCs without catalyst (Fig 2A). The intensity of signals at 1730 cm⁻¹ from the use of (Sn(Oct)₂ clearly increased (Fig 2E) as compared to organic catalysts such as DMAP (Fig 2D) and tartaric acid (Fig 2C), indicating that Sn(Oct)₂ was a more potent and selective catalyst in the toluene system. This result is opposed to what is known in the literature (Guo et al. 2013), which suggests that the copolymers synthesized using DMAP as the catalyst show significantly higher grafting levels of PCL than Sn(Oct)₂.

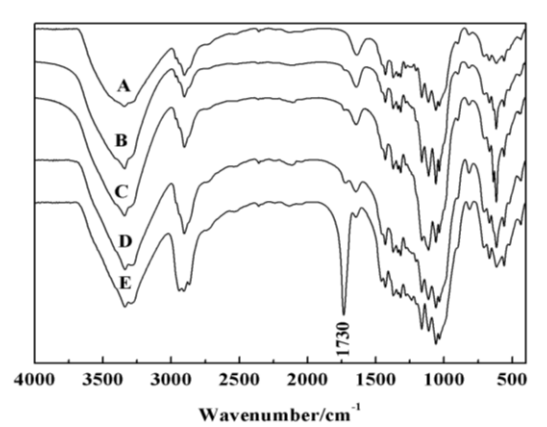


Fig 2 - The FT-IR spectra of CNCs and PCL-g-CNCs using different catalysts (A: CNCs; B: PCL-g-CNCs-non catalyst; C: PCL-g-CNCs-tartaric acid; D: PCL-g-CNCs-DMAP; E: PCL-g-CNCs-Sn(Oct)₂).

The catalytic effect is dependent on both the catalytic mechanism and reactivity of the catalyst. Sn(Oct)₂ is a coordination catalyst. It has been shown that Sn(Oct)₂ and hydroxyl in the initiator generated Sn-alkoxide bonds via a coordination-insertion mechanism, forming active centers for the propagation step (Coulembier et al. 2006). ROP was proposed to occur through a monomeractivated mechanism using DMAP as catalyst. The monomer-activation mechanism was proposed to occur by nucleophilic attack by DMAP on ε-CL to generate an alkoxide/acyl pyridinium zwitterion. Subsequent proton transfer from the hydroxyl on the surface of CNCs, followed by acylation of the resultant alkoxide, generated hydroxy-terminated ring-opened monomer. Polymerization proceeds by reaction of the hydroxyl group (Nederberg et al. 2001). It was reported that the molecular structure of ε-CL was more favorable to the nucleophilic attach than the coordination insertion (Kamber et al. 2007). The reaction was run in a toluene suspension. The solubility of Sn(Oct)2 was much higher than that of DMAP and tartaric acid. Thus, Sn(Oct)₂ could form more active centers with active centers for the propagation step. Meanwhile, the tartaric acid tertiary hydroxyl group competed with hydroxyl groups on the surface of CNCs to initiate polymer chains, reducing the grafted amount of PCL. Thus, the catalytic effect of Sn(Oct)₂ was superior to the other two catalysts.

Fitting of the model data

RSM is an empirical modeling technique for the analysis of the relationship of a series of controlled experimental factors and results. Here, the data of BBD were analyzed using Minitab 16 software to provide analysis of variance (ANOVA), regression coefficients, and regression. A regression equation for different monomer contents, polymerization temperatures, and times was obtained after ANOVA. All terms regardless of their significance are included in the following fitted second-order polynomial equation (Eq 4):

$$Y = -421.230 + 18.8228x_1 + 5.54133x_2 + 3.9421x_3 - 0.79113x_1^2 - 0.0217x_2^2 - 0.0715x_3^2 + 0.0263x_1x_2 + 0.0135x_1x_3 - 0.0027x_2x_3$$

The coefficients of above equation are calculated and the values are listed in *Table 3*.

P-value denoted the significance of the coefficients in *Table 3*. Coefficient of determination, R, is defined as the correlation between the observed and predicted values and is a measure of the goodness of fit. Joglekar and May (1987) suggested that for a good fit of a model, R² should be at least 0.80. That meant the regression models

explained the reaction well when the R²s are higher than 0.8. In this model, the R value was 99.79%, when R (predicted) was 96.90% and R (adjusted) was 99.41%. The value of R was close to R (adjusted), indicating that the fit of this model was very satisfactory. Meanwhile, the value of R was a little higher than R (predicted), demonstrating that the predictive nature of this model was credible.

Table 4 shows the results of RSM model fitting in the form of ANOVA. ANOVA analysis subdivides the total variation of all data into component parts associated with specific sources of variances in order to test hypotheses on the parameters of the model (Segurola et al. 1999). Model summary statistics in Table 2 represents the adequacy of models including linear, quadratic, and 2-factor interactions. As the F value of the modal is 262.67, and the P value of the modal is lower than 0.05, it is suggested that the model is highly significant. Meanwhile, the lack of fit, which is used to test the adequacy of the model, indicates that the P value of 0.137 is much higher than the significance level (0.05). It is suggested that there is no abnormality present in the diagnoses of residuals. Thus, it can be concluded that the model is statistically adequate.

Statistical analysis

It is important for the overall significance of the model to study the pattern of the mutual interactions between the variables. The model P value for the grafting ratio in $Table\ 3$ implies the significance of each variable in this value. When the P-value is less than 0.05, model terms are considered to be significant. As shown in $Table\ 3$, X_1 , X_2 , X_3 , $X_1 \times X_1$, $X_2 \times X_2$, $X_3 \times X_3$, and $X_1 \times X_2$ had a significant effect on the grafting ratio, because the P-values of these variables were less than 0.05. The T value is used to determine the significance of the regression

Table 3 - Coefficients of regression and confirmation.

Variable	Coefficient	Standard deviation	Т	Р	
Constant	122.46	1.5931	76.868	<0.001	
X_1	24.413	0.9756	25.023	< 0.001	
X_2	20.323	0.9756	20.831	< 0.001	
X ₃	4.49	0.9756	4.602	0.006	
$X_1 \times X_1$	-50.633	1.436	-35.259	< 0.001	
$X_2 \times X_2$	-8.683	1.436	-6.046	0.002	
$X_3 \times X_3$	-10.298	1.436	-7.171	0.001	
$X_1 \times X_2$	4.205	1.3797	3.048	0.028	
$X_1 \times X_3$	1.3	1.3797	0.942	0.389	
$X_2 \times X_3$	-0.65	1.3797	-0.471	0.657	
R = 99.79% R (predicted) = 96.90% R (adjusted) = 99.41%					

Table 4 - Results of RSM model fitting in the form of analysis of ANOVA.

Source	Degree of freedom (df)	Sum of squares(SS)	Mean squares(MS)	F-value	Р
Modal	9	18000.3	2000.03	262.67	<0.001
Liner	3	8233.1	2744.36	360.43	< 0.001
Square	3	9688.1	3229.35	424.12	< 0.001
Interaction	3	79.2	26.39	3.47	0.107
Residual error	5	38.1	7.61		
Lack of fit	3	34.5	11.50	6.45	0.137
Total	14	18038.4			

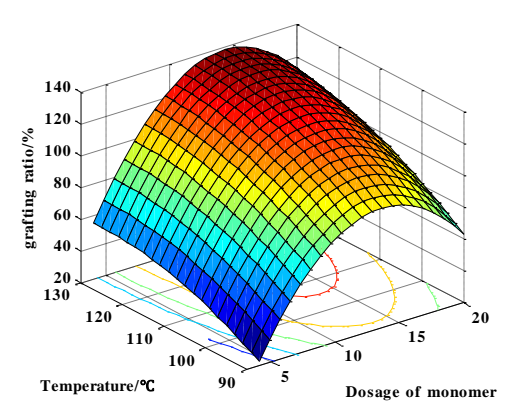


Fig 3 - Monomer content and polymerization temperature surface and contour of predicted grafting ratio (polymerization time = 24 h).

coefficients of the parameters, while the P values are used to check the significance of each interaction among the variables. It was reported that a more significant corresponding coefficient term could be obtained with the larger the magnitude of T and smaller value of P (Fu et al. 2007). The T value of the variables and their corresponding P shown in *Table 3* suggested that monomer content (T = 25.023, P < 0.001) produced the largest effect on grafting ratio, while the effect of the polymerization time (T = 4.602, P = 0.006) is the lowest.

Response surface and contour plots analysis

Coefficients of each variable relates to the effect of each factor on the response. A positive value represents a favorable impact on the optimization, while a negative value indicates an adverse relationship between the factor and the response (Chopra et al. 2007). As shown in *Table 3*, it is obvious that in a linear response, all the independent variables including the monomer content (X_1) , polymerization temperature (X_2) , and time (X_3) have positive effects on the three responses of grafting ratio (Y). It is also shown that all the quadratic effects of X_1 , X_2 , and X_3 are negative for response Y. The interaction effects of X_2 and X_3 are also unfavorable while the other two interactions are favorable.

To study the interactions between the three reaction condition factors and obtain a combined effect of the factors on the response of grafting ratio, the response surfaces and contour plots were generated using MATLAB software and are shown in Fig 3-5. When the effects of two factors were plotted over their studied range, the other one was set at its coded value of zero level. The shapes of response surfaces and contour plots indicate the nature and extent of the interactions (Ma et al. 2009). The contour plots display a more elliptical nature with more prominent interactions between the two factors (Fig 3), while the contour plots show a circular nature with less prominent or negligible interactions (Fig 5). All the relationships among the three variables are not linear, although Fig 3 and Fig 4 show a nearly linear relationship of X_1 with X_2 and X_3 , displaying almost straight lines up to the relationship exhibited in the contour plots.

Seen from the response surfaces shown in Fig 3-5, the grafting ratio increased with an increase in monomer

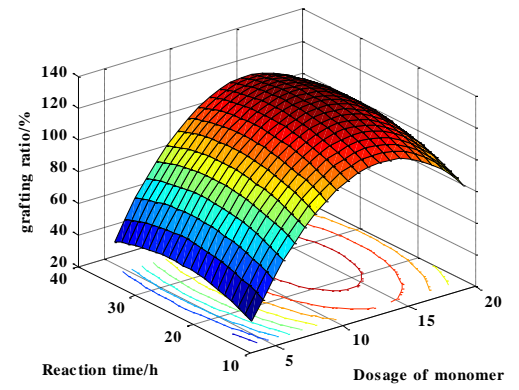


Fig 4 - Monomer content and polymerization time surface and contour of predicted grafting ratio (polymerization temperature: 110°C).

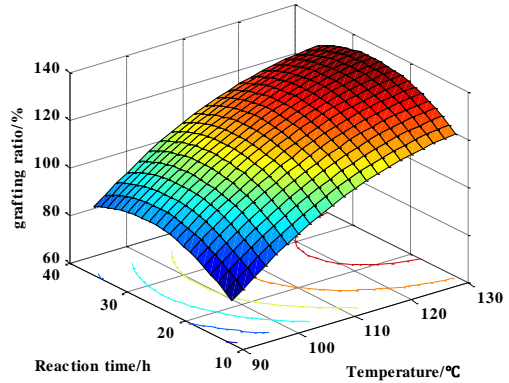


Fig 5 - Polymerization temperature and polymerization time surface and contour of predicted grafting ratio (monomer content: 12:1).

content at the middle levels, while a further increase in the level results in a gradual decrease in the response. ROP was initiated by the surface hydroxyl of CNCs. An excess of monomeric ϵ -CL was used and thus, there were not enough active centers (hydroxyls) to initiate the polymerization of CNCs and ε-CL. Consequently, sidereactions such as homo polymerization and transesterification occurred, ultimately affecting the grafting rate of PCL. The impact of polymerization time on grafting ratio was the same with monomer content, while its effect was much lower than that of the monomer content. There was almost a linear relationship between the grafting ratio and polymerization temperature, because the response continuously increased with an increase of temperature from 90°C to 130°C. It is in agreement with the work of Guo (Guo et al. 2013) and Carlmark (Carlmark et al. 2012) who showed higher temperature could favor the ROP reaction of cellulose with ε -CL. The activity of the catalyst increased with an increase in temperature thus promoting the grafting of PCL. But excess temperature also caused a lot of side reactions such as transesterification of ε-CL and degradation of PCL chains. When the temperature ranged from 90 to 130°C, the activity of the reaction system increased, and more PCL chains were grafted onto the CNCs. Although transesterification and degradation of monomer also occurred at this temperature, ROP was the dominant reaction pathway. Meanwhile, the solvent system used in this experiment was

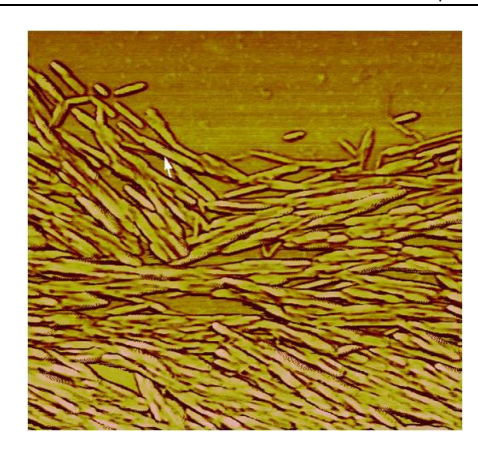


Fig 6 - Atomic force micrograph of CNCs (Scan area: 1×1µm²).

whose boiling point was 110°C. Too high of a temperature would cause severe bumping of toluene, so the maximum temperature chosen in this work was 130°C.

Optimization and verification

To determine the optimum factors for the maximum grafting ratio, optimal values of $Eq\ 3$ were determined by a Minitab-based numerical optimization. In the optimization study, optimum conditions are often calculated in the presence of constraints which ensure them to be more realistic (Bae et al. 2005). In this work, the upper limit of temperature was the most important constraint. Taking the constraints into consideration, the optimum operating parameters were found to be: $x_1 = 14:1$, $x_2 = 130^{\circ}$ C, and $x_3 = 26.5$ h. Under these conditions, the predicted maximum of grafting ratio was 138.57%.

To confirm the adequacy of the model for predicting the maximum grafting ratio, experiments were repeated three times using optimum conditions. The three replicate experiments obtained an average maximum grafting ratio of 134.23%, which approximated the predicted value. This result verified the validity of the model for optimizing the graft reaction conditions of PCL on CNCs using ROP. Meanwhile, it was further confirmed that the optimized conditions described in this study would be helpful for the mass-production of PCL-g-CNCs.

Surface morphology

Atomic force microscopy was used to characterize the surface morphology of CNCs used in this experiment. $Fig\ 6$ is the AFM image of CNCs with a scan area of $1\times1\mu\text{m}^2$. CNCs obtained from acid hydrolysis are rod-like, with a broad middle and sharp ends. They also show partial agglomeration. Diameter and length of CNCs shown in $Fig\ 6$ are 20~40 nm and 100~300 nm, respectively, suggesting that the size of CNCs is well within the nanometer scale. This result also corresponds to the literature that has reported the diameter of CNCs obtained from acid hydrolysis to be on the order of ~10-20 nm (Habibi et al. 2010).

FT-IR analysis

The success of grafting of PCL on CNCs was confirmed via FT-IR analysis. The FT-IR spectra of unmodified CNCs and PCL-g-CNCs with different monomer contents

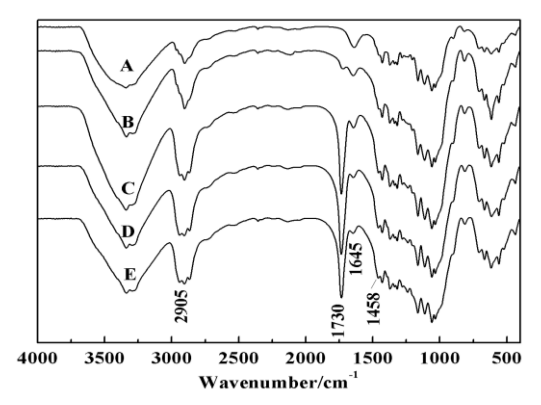


Fig 7 - FTIR spectra of CNCs and PCL-g-CNCs (A: CNCs; B: PCL-g-CNCs-4:1; C: PCL-g-CNCs-10:1; D: PCL-g-CNCs-14:1; E: PCL-g-CNCs-20:1).

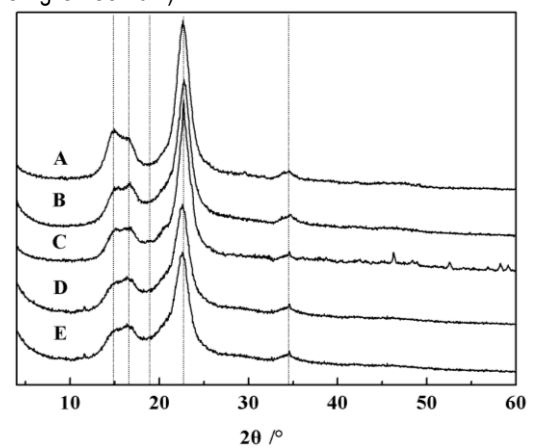


Fig 8 - XRD spectra of CNCs and PCL-g-CNCs (A: CNCs; B: PCL-g-CNCs-4:1; C: PCL-g-CNCs-10:1; D: PCL-g-CNCs-14:1; E: PCL-g-CNCs-20:1).

are displayed in Fig 7. The bands at 1734 cm⁻¹ (carbonyl group of esters) and 1458 cm⁻¹ (bending vibration of CH₂) are present in the spectra of the grafted samples, but absent in their unmodified precursors (Dong et al. 2008). With the increase of monomer content, more PCL was grafted onto CNCs, leading to enhancement of the intensities of these signals. Furthermore, the intensity of the signals at 1645 cm⁻¹ (bending vibration of -OH) weakened, indicating that more hydroxyls in CNCs reacted with ε-CL. Shoulder peaks at 2905 cm⁻¹ (C-H stretching of CH2) also appeared in the spectra of grafted samples. In order to confirm that these signals originated from the PCL grafted onto CNCs, not from the homo-PCL mixed with CNCs, all the samples were treated with dichloromethane extraction for 48 h to remove homo-PCL. It was found that a portion of the hydroxyls on the of CNCs initiated the ring opening polymerization of ε -CL and PCL had grafted onto CNCs.

XRD analysis

Fig 8 shows the XRD patterns of CNCs and PCL-g-CNCs with different monomer contents. The XRD spectra of unmodified CNCs (Fig 8A) displays well defined diffraction peaks at $2\theta = 14.8^{\circ}$, 16.5° , 22.8° and 34.5° , which correspond to the characteristic peaks of cellulose I. These characteristic peaks also appear in the diffractogram of PCL-g-CNCs, indicating that the polymerization does not change the main crystal structure

Table 5 - Degree of crystallinity determined from XRD for CNCs and PCL-g-CNCs.

0					
Samples		S	Degree of crystallinity (%)		
	Unmodified CNCs		77.8%		
	PCL-g-CNCs	4:1	77.1%		
	PCL-g-CNCs	10:1	75.9%		
	PCL-g-CNCs	14:1	71.2%		
	PCL-g-CNCs	20:1	74.0%		

of CNCs. But these peaks were less well-defined after the ROP reaction, probably due to the formation of a grafted layer at the surface of CNCs. Furthermore, characteristic peaks of PCL, appeared at 21.3° theoretically, were not defined for PCL-g-CNCs because a strong diffraction peak due to cellulose I occurs in the same diffraction angle range (Habibi et al. 2008). It also illustrates that the structure of nanocellulose limits the crystallization of PCL, leading to the result that PCL appears in PCL-g-CNCs mainly as an amorphous structure.

The crystallinity degree of CNCs before and after modification was determined using JADE 5 software. Results are reported in Table 5. The crystallinity degree decreased slightly from 77.8% to 71.2% when the mass ratio of ε -CL and CNCs was 14:1. It probably indicates that the cellulose crystals have been slightly damaged by the grafting of PCL. This alteration may be explained by the fact that PCL appears in the polymer mainly as an amorphous structure and the surface of the cellulose nanocrystals should be highly grafted inducing a possible peeling effect of modified crystals (Siqueira et al. 2010).

Thermal characterization

TGA analysis was carried out to study the degradation of CNCs and PCL-g-CNCs with different monomer contents (Fig 9). Compared with CNCs, the residual char of PCL-g-CNCs was reduced by approximately 10% (Fig 9A and 9C). In order to study the course of the reduction, TGA of the bulk of free PCL formed from ROP was performed. Results showed that there was no residual char of PCL at a temperature of 400°C. It is suggested that the reduction of residual char of PCL-g-CNCs was caused by the degradation PCL chains grafted onto the surface of CNCs. The weight loss at the temperature of 150°C could be attributed to the water absorption of the samples. It was obvious that the water content of PCL-g-CNCs was much

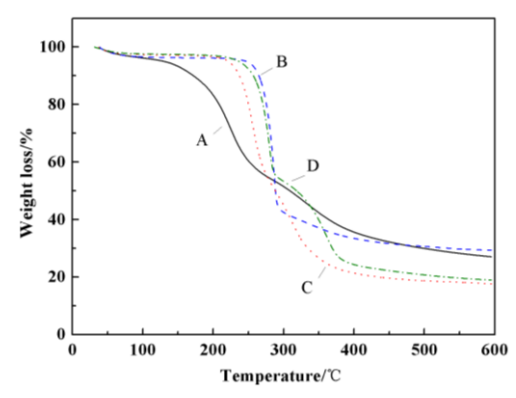


Fig 9 - TGA curves of CNCs and PCL-g-CNCs (A: CNCs; B: PCL-g-CNCs-4:1; C: PCL-g-CNCs-14:1; D: PCL-g-CNCs-20:1).

lower than CNCs, indicating that the hydrophobicity of CNCs increased after modification.

There are two decomposition processes observed in both the TGA curves of CNCs and PCL-g-CNCs (Fig 9A, 9C and 9D). However, the reasons for the two decomposition processes of CNCs and PCL-g-CNCs are different. Two broad peaks could be observed in the DTG curve of CNCs (Fig 10A). The maximum degradation rate temperature (T_{max}) of the first process was 227°C. This is an acid-catalyzed pyrolysis of CNCs (Wang et al. 2007). CNCs used in this experiment were obtained from acid hydrolysis. Acid sulfate groups retained in the CNCs could catalyze primary dehydration processes in cellulose chain units at lower temperatures. This degradation then spread to the cellulose crystal interiors, which were not in direct contact with the catalyst, forming a solid residue (Kim et al. 2001). Then the second process occurred at a higher temperature of 344°C, with slow decomposition of solid residues to form the char products.

PCL-g-CNCs also had two decomposition processes. The T_{max} of the first process of PCL-g-CNCs was higher than that of the CNCs (Fig 10). After neutralization with a NaOH solution, the catalysis of acid sulfate groups was eliminated and the first process of PCL-g-CNCs shifted to higher temperature (>280°C in Fig 10). So the first decomposition peak may be attributed to the degradation of cellulose. Compared with PCL-g-CNCs 14:1 and PCLg-CNCs-20:1, the second decomposition peak of PCL-g-CNCs-4:1 (Fig 10B) was inconspicuous, due to the disappearance of acid sulfate groups and the small grafting amount of PCL. Meanwhile, T_{max} of the second process of PCL-g-CNCs-14:1 and PCL-g-CNCs-20:1 (Fig 10C and 10D) was obvious and higher than that of the CNCs, indicating that the second decomposition peak of PCL-g-CNCs was due to the decomposition of PCL side chains.

XPS analysis

XPS analysis was used to confirm the presence of PCL polymers after grafting. Low resolution spectra of CNCs and PCL-g-CNCs showed that carbon and oxygen atoms are the main atomic constituents (*Fig 11A*). After modification, the ratio of carbon atoms in the sample increased. In the high-resolution carbon spectra (*Fig 11B and 11C*), the carbon signal can be resolved into four component peaks (Labet et al. 2011): the C1 contribution

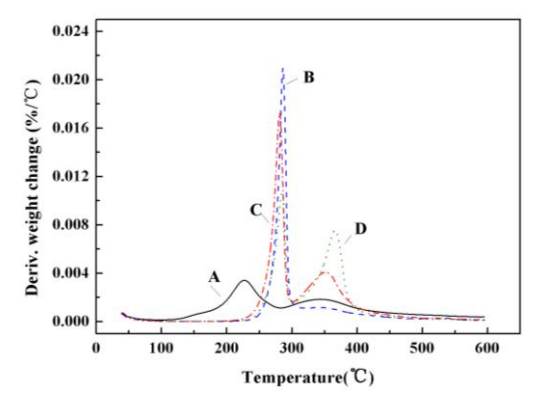


Fig 10 - DTG curves of CNCs and PCL-g-CNCs (A: CNCs; B: PCL-g-CNCs-4:1; C: PCL-g-CNCs-14:1; D: PCL-g-CNCs-20:1)

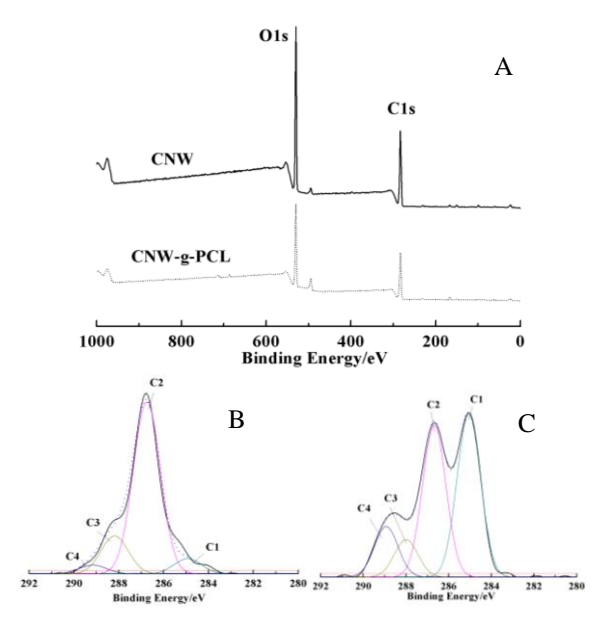


Fig 11 - XPS spectra of CNCs and PCL-g-CNCs (A: wide scan spectra; B: deconvolution of the C1s peak of CNCs; C: deconvolution of the C1s peak of PCL-g-CNCs).

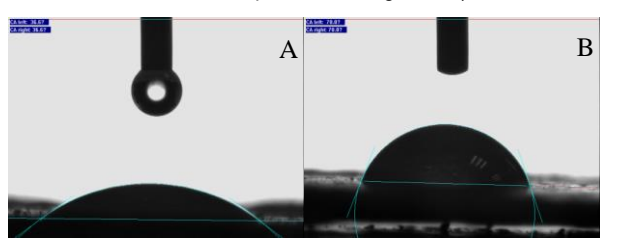


Fig 12 - Sessile contact angle images of CNCs and PCL-g-CNCs (A: CNCs; B: PCL-g-CNCs).

Table 6 - Surface carbon atoms proportions obtained from the deconvolution of the C1s peak, XPS analysis.

	C-C/C- H (%)	C-O (%)	O-C-O (%)	O-C=O (%)
Bonding Energy (eV)	285.0	286.6	288.0	289.0
CNCs	6.59	74.68	16.45	3.75
PCL-g-CNCs	40.70	38.91	7.89	11.95

(285.0 eV) corresponds to the C-C or C-H bonds; the C2 contribution (286.5 eV) corresponds to the C-O bonds; the C3 contribution (288.0 eV) corresponds to the O-C-O bonds; and the C4 contribution (289.0 eV) corresponds to the bonds. In both CNCs and PCL-g-CWS samples, the four component peaks can be therefore categorized by the kind of C bonds involved in PCL and nanocellulose structures. The four types of carbon atoms were all present in the spectra of nanocellulose before and after grafting, but the proportions of each carbon atom were different (Table 6). The atom concentrations of different C bonds were calculated from the peak areas of each C peak, using Gaussian deconvolution. In CNCs sample, the high proportion of C-O can be explained by the C-O-C in the glucose ring and the C-OH of the glucose ring, while the C3 contribution is corresponding to the O-C-O bonds in the glucose ring. But the appearance of O-C=O can be only attributed to the residual reducing end forming from acid hydrolysis, and the presence of C–C can be ascribed to the residual impurities at the surface of CNCs. The ratio of O–C–O to C–O–C is 0.22 for CNCs. This value is very close to the theoretical value of 0.2 calculated from pure cellulose (Habibi et al. 2008).

After grafting, the proportions of each carbon atoms were very different. The proportions of C–C and O–C=O in PCL-g-CNCs clearly increased. This increase can be explained by the aliphatic chains and ester function of PCL. C–O also appears with a decreased proportion. Its appearance can be attributed to the hydroxyl end of PCL besides of the C–O–C and unmodified C–OH in the glucose rings. These changes of carbon atoms in PCL-g-CNCs indicate that the surface of CNCs is covered with PCL chains.

Contact angle measurements

Static contact angle measurements were used to estimate the degree of hydrophobicity of PCL-g-CNCs. Contact angles of CNCs and PCL-g-CNCs with water are shown in Fig 12. In this measurement, unmodified CNCs adsorbed water very quickly displaying a low contact angle of 36.6°. However, PCL-g-CNCs after ROP adsorbed water slowly to display a contact angle of 70.0°. A clear and significant increase of the contact angle is therefore observed between the unmodified CNCs (Fig 12A, CA = 36.6°) and the PCL-g-CNCs (Fig 12B, CA = 70.0°). The initial contact angle value is about twice that of ungrafted CNCs after grafting PCL. CNCs before modification were therefore completely hydrophilic. A considerable increase in the hydrophobicity of PCL-g-CNCs was clearly demonstrated by the corresponding increase in contact angles with water. This increase in contact angle for the modified CNCs is ascribed to the coverage of CNCs by a hydrophobic polymeric brush (Labet et al. 2007). Comparing the contact angle value obtained for unmodified CNCs to those obtained for modified CNCs, it is apparent that a surface chemical modification successfully occurred.

Conclusions

CNCs have been successfully grafted with PCL by ROP (ring-opening polymerization). Solvent-exchange was chosen as the CNCs pretreatment method and Sn(Oct)₂ was chosen as the catalyst in these experiments. A response surface methodology using Box-Behnken design was employed to investigate the effect of ROP operation conditions. The optimum operating conditions were an ε-caprolactone to CNCs ratio (monomer content) of 14:1, a polymerization temperature of 130°C, a polymerization time of 26.5 h, with a maximum predicted grafting ratio of 138.57%. The synthesis was confirmed by FT-IR, XRD, TGA, XPS, and contact angle analysis. The obtained PCL-g-CNCs demonstrated significantly different functional groups, carbon atom proportions, and thermal properties from their precursors. XRD analysis showed that the polymerization did not change the main crystal structure of CNCs despite the appearance of the PCL characteristic peaks, while the contact angle increased from 36.6° to 70° after polymerization to support the hydrophobic nature of the CNCs after modification.

Acknowledgements

The financial support of the National Natural Science Foundation of China (No. 31170549) and the Major State Basic Research Development Program (No.2010CB732206) are gratefully acknowledged. We are also grateful for a China-US Scholar Exchange Program administered through SCUT that facilitated parts of this work.

Literature

- **Açıkel, Ü., Erşan, M. and Açıkel, Y.S.** (2010): Optimization of critical medium components using response surface methodology for lipase production by Rhizopusdelemar. Food Bioprod. Process., 88(1):31-39.
- **Bae, S. and Shoda, M.** (2005): Statistical optimization of culture conditions for bacterial cellulose production using Box-Behnken design. Biotechnology and Bioengineering, 90 1, 20-28.
- **Cao, X.D., Habibi, Y. and Lucia, L.A.** (2009): One-pot polymerization, surface grafting, and processing of waterborne polyurethane-cellulose nanocrystal nano-composites, J. Mater. Chem., 19, 7137-7145.
- Carbone, C., Tomasello, B., Ruozi, B., Renis, M. and Puglisi, G. (2012): Preparation and optimization of PIT solid lipid nanoparticles via statistical factorial design. European Journal of Medicinal Chemistry, 49, 110-117.
- **Carlmark, A., Larsson, E. and Malmström, E.** (2012): Grafting of cellulose by ring-opening polymerisation A review. European Polymer Journal, 48, 1646-1659.
- Chopra, S., Motwani, S.K., Iqbal, Z., Talegaonkar, S., Ahmad, F.J. and Khar, R. K. (2007): Optimisation of polyherbal gels for vaginal drug delivery by Box-Behnken statistical design, European Journal of Pharmaceutics and Biopharmaceutics, 67, 120-131.
- Coninck, J.D., Bouquelet, S., Dumortier, V., Duyme, F., and Denantes, I.V. (2000): Industrial media and fermentation processes for improved growth and protease production by Tetrahymena thermophila BIII, Journal of Industrial Microbiologyand Biotechnology, 24(4), 285-290.
- Coulembiera, O., Dege´e, P., Hedrickb, J.L., and Dubois, P. (2006): From controlled ring-opening polymerization to biodegradable aliphatic polyester: Especially poly(b-malic acid) derivatives, Prog. Polym. Sci., 31, 723-747.
- Dong, H., Xu, Q., Li, Y., Mo, S., Cai, S. and Liu, L. (2008): The synthesis of biodegradable graft copolymer cellulose-graft-poly(I-lactide) and the study of its controlled drug release, Colloids and Surfaces B: Biointerfaces, 66(1), 26-33.
- **Dong, X.M., Revol, J-F.O. and Gray, D.G.** (1998): Effect of microcrystallite preparation conditions on the formation of colloid crystals of cellulose, Cellulose, 5, 19-32.
- **Dufresne, A.** (2003): Interfacial phenomena in nanocomposites based on polysaccharide nanocrystals, Composite Interfaces, 10, 369-387.
- **Fu, J.F., Zhao, Y.Q. and Wu, Q.L.** (2007): Optimising photoelectron catalytic oxidation of fulvic acid using response surface methodology, Journal of Hazardous Materials, 144, 499-505.
- **Ghanem, K.M., Al-Garni, S.M. and Al-Shehri, A.N.** (2009): Statistical optimization of cultural conditions by response

- surface methodology for phenol degradation by a novel Aspergillus flavus isolate. African Journal of Biotechnology, 8(15), 3576-3583.
- **Goffin, A.L., Habibi, Y., Raquez, J.M. and Dubois, P.** (2012): Polyester-grafted cellulose nanowhiskers: a new approach for tuning the microstructure of immiscible polyester blends,. ACS Appl. Mater. Interfaces, 4, 3364-3371.
- Goffin, A.L., Raquez, J.M., Duquesne, E., Siqueira, G., Habibi, Y., Dufresne, A. and Dubois, P. (2011a): From Interfacial Ring-Opening polymerization to Melt Processing of cellulose nanowhisker-filled polylactide-based nanocomposites, Biomacromolecules, 12, 2456-2465.
- Goffin, A.L., Raquez, J.M., Duquesne, E.,Siqueira, G., Habibi, Y., Dufresne, A. and Dubois, P. (2011b): Poly(e-caprolactone) based nanocomposites reinforced by surface-grafted cellulose nanowhiskers via extrusion processing: morphology, rheology, and thermo-mechanical properties, Polymer, 52, 1532-1538.
- **Guo, Y.Z., Wang, X.H., Shen, Z.G., Shu, X.C. and Sun, R.C.** (2013): Preparation of cellulose-graft-poly(ε-caprolactone) nanomicelles by homogeneous ROP in ionic liquid, Carbohydrate Polymers, 92, 77-83.
- **Habibi, Y. and Dufresne, A.** (2008): Highly filled bionanocomposites from functionalized polysaccharide nanocrystals, Biomacromolecules, 9, 1974-1980.
- **Habibi, Y., Lucia, L.A. and Rojas, O.J.** (2010): Cellulose nanocrystals: chemistry, self-Assembly, and applications, Chem. Rev., 110, 3479-3500.
- Habibi, Y., Schiltz, N., Duquesne, E., Dubois, P. and Dufresne, A. (2008):Bionanocomposites based on poly(3-caprolactone)-grafted cellulose nanocrystals by ring-opening polymerization, J. Mater. Chem., 18, 5002-5010.
- Hadidi, N., Kobarfard, Farzad., Nafissi-Varcheh, N. and Aboofazeli, R. (2011): Optimization of single-walled carbon nanotube solubility by noncovalent PEGylation using experimental design methods, International Journal of Nanomedicine, 6, 737-746.
- **Hafrén, J. and Cordova, A.** (2005): Direct organo catalytic polymerization from cellulose fibers, Macromol Rapid Commun, 26(2), 82-86.
- Hajji, M., Rebai, A., Gharsallah, N. and Nasri, M. (2008): Optimization of alkaline protease production by Aspergillus clavatus ES1 in Mirabilis jalapa tuber powder using statistical experimental design, Appl Microbiol Biotechnol, 79, 915-923.
- He, J.X., Cui, S.Z., and Wang, S.Y. (2008): preparation and crystalline analysis of high-grade bamboo dissolving pulp for cellulose acetate, 107, 1029-1038.
- Imandi, S.B., Bandaru, V.V., Somalanka, S.R., Bandaru, S.R. and Garapati, H.R. (2008): Application of statistical experimental designs for the optimization of medium constituents for the production of citric acid from pineapple waste, Bioresource Technology, 99(10), 4445-4450.
- **Jiang, F., Esker, A.R. and Roman, M.** (2010): Acid-catalyzed and solvolyticde desulfation of H₂SO₄-hydrolyzed cellulose nanocrystals, Langmuir, 26(23), 17919-17925.
- **Joglekar, A.M. and May, A.T.** (1987): Product excellence through design of experiments, Cereal Foods World, 32, 857-868.

- Kamber, N.E., Jeong, W. and Waymouth, R.M. (2007): Organocatalytic Ring-Opening Polymerization, Chem. Rev. 107, 5813-5840.
- **Kim, D-Y., Nishiyama, Y., Wada, M. and Kuga, S.** (2001): High-yield carbonization of cellulose by sulphuric acid impregnation, Cellulose, 8(1), 29-33.
- **Klemm, D., Heublein, B., Fink, H-P.and Bohn, A.** (2005): Cellulose: fascinating biopolymer and sustainable raw material, Angew. Chem. Int. Ed, 44(22), 3358-3393.
- Korhonen, J.T., Hiekkataipale, P., Malm, J., Karppinen, M., Ikkala, O. and Ras, R.H.A. (2011): Inorganic hollow nanotube aerogels by atomic layer deposition onto native nanocellulose templates, ACS Nano, 5 (3), 1967-1974.
- **Labet, M. and Thielemans, W.** (2011): Improving the reproducibility of chemical reactions on the surface of cellulose nanocrystals: ROP of epsilon-caprolactone as a case study. Cellulose, 18(3), 607-617.
- **Labet, M., Thielemans, W. and Dufresne, A.** (2007): Polymer grafting onto starch nanocrystals, Biomacromolecules, 8, 2916-2927.
- **Liu, X., Chen, J., Sun, P., Liu, Z.W. and Liu, Z.T.** (2010): Grafting modification of ramie fibers with poly(2,2,2-trifluoroethyl methacrylate) via reversible addition fragmentation chain transfer (RAFT) polymerization in supercritical carbon dioxide. Reactive & Functional Polymers, 70(12), 972-979.
- **Lönnberg**, **H.**, **Fogelström**, **L.**, **Berglund**, **M.A.S.A.S.L.**, **Malmström**, **E. and Hult**, **A.** (2008): Surface grafting of microfibrillated cellulose with poly(e-caprolactone)-synthesis and characterization, European Polymer Journal, 44 2991-2997.
- Ma, H., Liu, W.W., Chen, X., Wu, Y.J. and Yu Z.L. (2009): Enhanced enzymatic saccharification of rice straw by microwave pretreatment, Bioresource Technology, 100, 1279-1284.
- Mohana, S., Shrivastava, S., Divecha, J.and Madamwar, D. (2008): Response surface methodology for optimization of medium for decolorization of textile dye Direct Black 22 by a novel bacterial consortium. Bioresource Technology, 99(3), 562-569.
- **Morandi, G., Heath, L., and Thielemans, W.** (2009): Cellulose nanocrystals grafted with polystyrene chains through Surface Initiated Atom Transfer Radical Polymerization (SI-ATRP), Langmuir, 25(14), 8280-8286.
- **Nederberg, F., Conno,r E,F., Möller, M., Glauser, T. and Hedrick J.L.** (2001): New paradigms for organic catalysts: the first organocatalytic living polymerization, Angew. Chem. Int. Ed., 40(14), 2712-2715.
- Peng, X.W., Ren, J.L., Zhong, L.X. and Sun R.C. (2011): Nanocomposite films based onxylan-rich hemicelluloses and

- cellulose nanofibers with enhanced mechanical properties, Biomacromolecules, 12, 3321-3329.
- **Roman, M. and Winter, W.T.** (2006): Cellulose nanocomposites: processing, characterization and properties, ACS Symposium Series, 938, 99-113.
- Samir, M., Alloin, F. and Dufresne, A. (2005): Review of recent research into cellulosic whiskers, their properties and their application in nanocomposite field, Biomacromolecules, 6(2), 612-626.
- **Segurola, J., Allen, N.S., Edge, M. and Mahon, A.M.** (1999): Design of eutectic photoinitiator blends for UV/curable curable acrylated printing inks and coatings, Prog. Org. Coa, 37, 23-37.
- Siala, R., Frikha, F., Mhamdi, S., Nasri, M. and Kamoun, A.S. (2012): Optimization of acid protease production by aspergilla using erl1 on shrimp peptone using statistical experimental design, The Scientific World Journal, 1-11.
- **Siqueira, G., Bras, J. and Dufresne, A.** (2010): New process of chemical grafting of cellulose nanoparticles with a long chain isocyanate, Langmuir, 26(1), 402-411.
- Vitorino, C., Carvalho, F.A., Almeida, A.J., Sousa, J.J. and Pais, A.A.C.C. (2011): The size of solid lipid nanoparticles: an interpretation from experimental design, Coll. Surf. B, 84, 117-130
- Wang, J.P., Chen, Y.Z., Wang, Y., Yuan, S.J. and Yu, H.Q. (2011): Optimization of the coagulation-flocculation process for pulpmill wastewater treatment using a combination of uniform design and response surface methodology, Water research, 45, 5633-5640.
- Wang, N., Ding, E. and Cheng, R. (2007): Thermal degradation behaviors of spherical cellulose nanocrystals with sulfate groups, Polymer, 48, 3486-3493.
- Wang, Y.X., Tian, H.F. and Zhang, L.N. (2010): Role of starch nanocrystals and cellulose whiskers in synergistic reinforcement of waterborne polyurethane, Carbohydrate Polymers, 80, 665-671.
- **Wu, Q.J., Henriksson, M., Liu, X.H. and Berglund, L.A.** (2007): A high strength nanocomposite based on microcrystalline cellulose and polyurethane, Biomacromolecules, 8(12), 3687-3692.
- Zhou, J.Y., Yu, X.J., Ding, C., Wang Z.P., Zhou, Q.Q., Pao, H. and Cai, W.M. (2011): Optimization of phenol degradation by Candida tropicalis Z-04 using Plackett-Burman design and response surface methodology, Journal of Environmental Sciences, 23(1), 22-30
- Zhou, Y.M., Fu, S.Y., Zheng, L.M. and Zhan, H.Y. (2012): Effect of nanocellulose isolation techniques on the formation of reinforced poly(vinyl alcohol) nanocomposite films, eXPRESS Polymer Letters, 6, (10), 794-804.
 - Manuscript received October 24, 2013 Accepted January 21, 2014